JACS
JOURNAL OF THE AMERICAN CHEMICAL SOCIETY
Article
pubs.acs.org/JACS

Rational Design of Porous Conjugated Polymers and Roles of Residual Palladium for Photocatalytic Hydrogen Production

Lianwei Li,[†] Zhengxu Cai,[†] Qinghe Wu,[†] Wai-Yip Lo,[†] Na Zhang,[†] Lin X. Chen,[‡,§] and Luping Yu*[,†]

[†]Department of Chemistry and the James Franck Institute, The University of Chicago, 929 East 57th Street, Chicago, Illinois 60637, United States

[‡]Chemical Sciences and Engineering Division, Argonne National Laboratory, 9700 South Cass Avenue, Lemont, Illinois 60439, United States

[§]Department of Chemistry, Northwestern University, 2145 Sheridan Road, Evanston, Illinois 60208, United States

Supporting Information

ABSTRACT: Developing highly efficient photocatalysts for water splitting is one of the grand challenges in solar energy conversion. Here, we report the rational design and synthesis of porous conjugated polymer (PCP) that photocatalytically generates hydrogen from water splitting. The design mimics natural photosynthetics systems with conjugated polymer component to harvest photons and the transition metal part to facilitate catalytic activities. A series of PCPs have been synthesized with different light harvesting chromophores and transition metal binding bipyridyl (bpy) sites. The photocatalytic activity of these bpy-containing PCPs can be greatly enhanced due to the improved light absorption, better wettability, local ordering structure, and the improved charge separation process. The PCP made of strong and fully conjugated donor chromophore DBD (M_4) shows the highest hydrogen production rate at ~33 μmol/h. The results indicate that copolymerization between a strong electron donor and weak electron acceptor into the same polymer chain is a useful strategy for developing efficient photocatalysts. This study also reveals that the residual palladium in the PCP networks plays a key role for the catalytic performance. The hydrogen generation activity of PCP photocatalyst can be further enhanced to 164 μmol/h with an apparent quantum yield of 1.8% at 350 nm by loading 2 wt % of extra platinum cocatalyst.

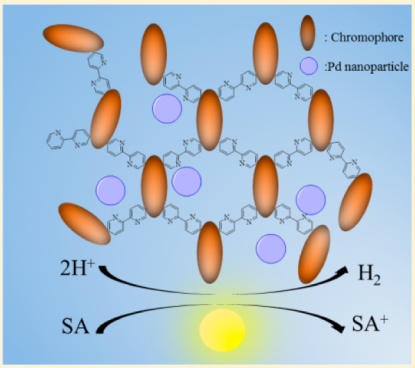

INTRODUCTION

Water splitting into hydrogen and oxygen is an uphill reaction, requiring a driving force of >1.23 eV and multiple redox equivalents.[1−3] Although the abundant solar energy seems to be a natural choice for driving chemical reactions and to store energy as fuels, it is a huge challenge to couple multiple single photon absorption to multiple redox equivalent generation. To circumvent this challenge, semiconductors for photocatalytic hydrogen production (PHP) from water (half-reaction of water splitting) have been developed in recent years for these materials are capable of absorbing multiple photons, possessing high carrier mobility, and catalytic functions.[1−3] In comparison, organic semiconductors have scarcely been investigated for this purpose, although they also exhibit attractive ability to absorb multiple photons, reasonable carrier mobility, and more importantly diverse synthetic modularity for tailing their properties. So far, there are only a handful of organic semiconductor systems disclosed in the literature.[4−18] A well-known all-organic system for photocatalytic water splitting is graphitic carbon nitride (g-C_3N_4)-based materials, first reported by Antonietti and co-workers in 2009.[4] Although pure g-C_3N_4 showed negligible activity, significant increases in the rate of hydrogen production were achieved by modifying g-C_3N_4 by morphology control, donor−acceptor copolymerization, and doping processes.[5−9] Various analogues of g-C_3N_4, such as poly(azomethines)-,[10] poly(triazine)-,[11] poly(heptazine)-,[12] and poly(hydrazine)-based networks,[13] are developed. A linear poly(*p*-phenylene) system[14,15] has also been studied for its PHP function. Very recently, Cooper and co-workers reported that a pyrene-based conjugated microporous polymer was an efficient photocatalyst for water reduction.[16]

Multiple factors can influence the PHP efficiency, including light absorption, charge separation, charge transport, and surface chemical reactions. Thus, careful control and detailed understanding in the optical band gap, HOMO−LUMO energy levels, energy level offset between the LUMO energy level and the H_2O/H_2 redox potential (thermodynamic driving force), charge carrier mobility, surface area, and interface wettability are crucial to obtain efficient photocatalysts. Our group has been pursuing PCP research and applications on catalysis for a long time[19−22] such as oxygen reduction reactions.[22] This Article describes our effort in rationally designing PCP for photocatalytic hydrogen production from water, which has been expanded from our success in designing low band gap polymers for photovoltaic devices. Several chromophore

Received: April 5, 2016
Published: June 2, 2016

DOI: 10.1021/jacs.6b03472
J. Am. Chem. Soc. 2016, 138, 7681−7686

monomers were copolymerized with biphenyl (bph) and bipyridyl (bpy) comonomers to generate the target PCPs through palladium-mediated polycondensation (Figure 1). By

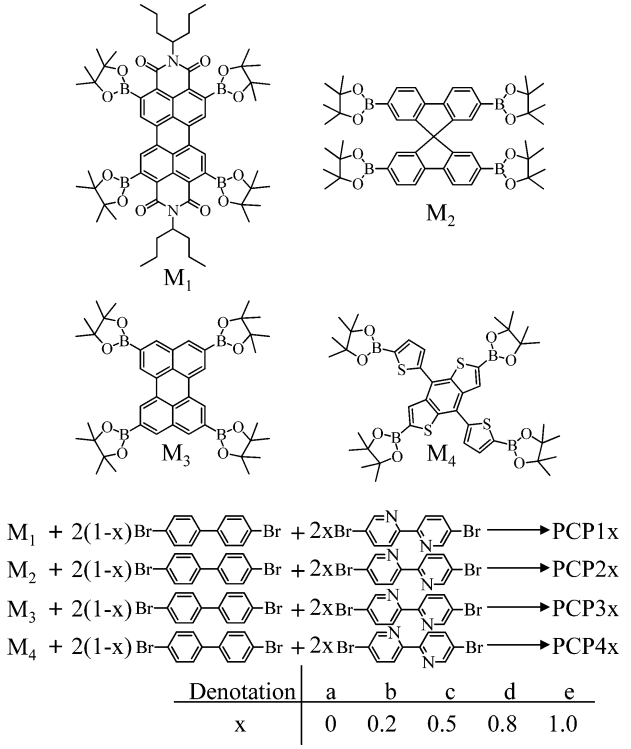

Figure 1. Structures of monomers and synthesis of PCP photocatalysts by Suzuki polycondensation.

varying chemical structures of the chromophore monomers from strong electron acceptors to strong electron donors and changing the biphenyl/bipyridyl copolymerization ratio, a series of PCPs with varied physical and chemical properties were synthesized. Detailed syntheses and their photocatalytic performances for hydrogen production from water in the presence of a sacrificial electron donor are described in this Article.

RESULTS AND DISCUSSION

Synthesis and Characterization of PCPs. In our past research effort on designing highly efficient organic photovoltaic (OPV) polymers for solar cells, we learned that intrachain charge transfer character and direction are important in defraying excitons binding energy and assisting exciton dissociation and charge generation.[23−25] The idea for designing PCPs is based on the same rationality for generating holes and electrons from exciton splitting for water reduction. Furthermore, to effectively transport charge to reaction sites, polymer backbones must contain conjugated systems that support charge transport. Therefore, two types of monomers, electron-deficient (M_1) and electron-rich chromophores (M_2−M_4), were synthesized. To investigate the structure/property relationship of PCP photocatalysts, each of these monomers was copolymerized with the weak donor biphenyl (bph) and weak acceptor bipyridyl (bpy) comonomers at different ratios (Figure 1). The monomer M_4 is especially interesting because it provides a fully conjugated connection in multiple directions with either bph or bpy comonomer, which favors charge transport. The synthetic procedures for the monomers and PCPs are described in the Supporting Information. All of the PCP polymers were synthesized by copolymerization via Pd-catalyzed Suzuki polycondensation. To simplify the discussion, the prepared PCPs are named as PCP*y*a−e, where *y* = 1−4, and a, b, c, d, and e represent that the mole fraction of bpy monomer incorporated into networks is 0%, 20%, 50%, 80%, and 100%, respectively.

Because the polymers are cross-linked materials, they cannot be characterized with most of the traditional instrumentations. However, FTIR spectral, solid-state ^{13}C NMR spectral, and elemental analyses provide evidence for the chemical structures of these PCPs. FTIR spectra (Figure S1) show that the stretching vibration strength of C/N double bond in the bpy ring located at 1456 and 1563 cm^{-1} gradually increases as the bpy content increases for all of the PCP1−4, indicating the chemical composition of prepared PCPs was fine-tuned by changing the bph/bpy ratio. The solid-state ^{13}C NMR spectra of PCPya and PCPye polymers display broad peaks ranging from 100 to 170 ppm (Figure S2), corresponding to signals of aromatic carbons. The carbon signals from pyridine can be clearly observed at 152 ppm for all PCPye. The small peaks located at ∼25.0 ppm indicate the residual borate groups. Elemental analysis of PCPya and PCPye supports the structures as proposed (Table S1). TGA results indicate that most of the PCPs are thermally stable in air up to 250 °C (Figure S3).

Morphological Study. The porous property of PCPya and PCPye for PCP1−4 was investigated by nitrogen adsorption/desorption experiments at 77 K. The isotherms and pore size distribution curves obtained using the Brunauer−Emmett−Teller (BET) and Barrett−Joyner−Halenda (BJH) methods are summarized in Figures S4 and S5. The PCP2e shows the highest apparent $SA_{BET} \approx 279\ m^2/g$, while PCP1a shows the lowest due to the bulky side chains (Table 1). The nitrogen gas

Table 1. Physical and Chemical Properties and Hydrogen Production Rates of the PCP Photocatalysts

PCP	SA_{BET}[a] (m^2/g)	λ_o[b] (nm)	E_g[c] (eV)	Pd[d] (wt %)	$H_{2,ful}$[e] (μmol/h)	$H_{2,vis}$[e] (μmol/h)
PCP1a	39	683	1.81	1.22	1.4	0.06
PCP1e	59	633	1.95	1.60	13.0	0.49
PCP2a	228	429	2.89	1.15	6.4	1.39
PCP2e	279	505	2.45	0.89	26.0	5.11
PCP3a	121	535	2.31	1.17	5.1	0.91
PCP3e	99	566	2.19	0.94	17.8	2.75
PCP4a	80	530	2.33	0.84	7.2	1.45
PCP4e	104	601	2.06	0.81	33.0	6.65

[a]BET surface areas (SA_{BET}) were calculated from the N_2 adsorption isotherms from 0.005 to 0.20 bar. [b]The absorption onsets (λ_o) of these PCPs were measured by diffuse reflectance UV−vis spectroscopy. [c]The optical bandgaps were calculated by the equation $E_g = 1240/\lambda_o$. [d]The residual Pd contents were measured by ICP-MS. [e]$H_{2,ful}$ and $H_{2,vis}$ represent the hydrogen production rates under full-arc irradiation and visible light irradiation, respectively.

uptake at low relative pressure ($P/P_0 < 0.05$) reflects moderate microporous structure with pore size smaller than 2 nm. The observed hysteresis loop is caused by elastic deformation of the cross-linked network in the course of nitrogen sorption.[26] The sharp rise at high pressure regions (P/P_0 = 0.9−1.0) can be contributed to the presence of macropores (>50 nm) or absorbance at external surface area or textural porosity in these materials. Overall, the PCPs shown here are less porous than the PCPs that we reported previously, which is due to the bulky

DOI: 10.1021/jacs.6b03472
J. Am. Chem. Soc. 2016, 138, 7681−7686

molecular structures of chromophore units bearing alkyl side chains and the longer linker monomers.[20−22]

The morphology of the solid state of these PCPs was investigated by scanning electron microscopy (SEM). SEM images (Figure S6) show that all of the PCPa and PCPe have either globular or palette aggregates with dimensions on the submicrometer scale. All of the bpy-containing PCPe exhibit larger primary aggregation sizes as compared to their PCPa counterparts, which should be originated from the different solubility property and reaction kinetics of bph and bpy monomers.

The powder X-ray diffraction (Figure S7) patterns of PCP1−3 show broad and low intensity peaks ranging from 10° to 25° (2θ), suggesting that it is amorphous in nature for PCP1−3. In contrast, M_4-based PCPs were surprisingly found to show sharp and strong diffraction peaks at 18° (2θ), corresponding to a d-spacing of 4.8 A. This diffraction may be due to the ordered stacking of local two-dimensional segments. The peak intensity is much stronger for PCP4e as compared to PCP4a. The local ordering structure of PCP4 is beneficial for the charge transport due to its close $\pi-\pi$ stacking.

Optical Property and Energy Diagram of PCPs. To develop effective PCP photocatalysts, proper optical bandgaps and energy level alignments are required. The optical absorption profile and energy level alignment of the prepared PCPs were investigated by combining diffuse reflectance UV−vis spectroscopy, CV measurement, and DFT calculation.[8,11] The prepared PCPs show the appearance of the color ranging from white to dark red (Figure 2a). The absorption onset λ_o of

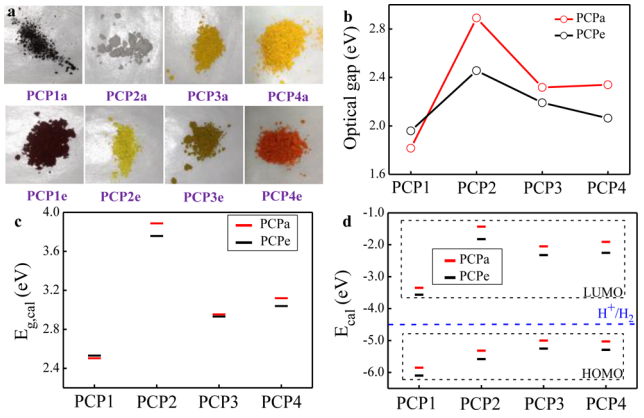

Figure 2. (a) Photographs of the prepared PCPa and PCPe photocatalysts. (b) Experimental optical bandgaps of PCPa and PCPe photocatalysts. (c) Calculated energy bandgaps of fragmental structures of PCPa and PCPe photocatalysts. (d) Calculated energy level diagram of fragmental structures of PCPa and PCPe photocatalysts, where the blue line represents the redox potential of H^+/H_2.

these PCPs ranges from 429 to 683 nm (Figure S8 and Table 1). The optical bandgap (E_g) values of these PCPs are shown in Table 1 and Figure 2b. PDI-based PCP1a shows the lowest $E_g \approx 1.81$ eV, while SBF-based PCP2a shows the widest $E_g \approx 2.89$ eV due to limited extension of conjugation caused by the twisted structures. Attempts to further determine the LUMO and HOMO energy levels of these PCPs, by using CV measurement with a drop-casting sample from an acetone suspension of PCP4e (4 mg) and Nafion (100 uL) onto ITO electrode, failed to reveal any meaningful data due to the poor contact of the insoluble PCP and the electrode.

DFT calculations of the fragmental structures of PCP networks (Figure S9) were carried out to gain insightful information not only about the trend of energy bandgaps, but also about the relative HOMO and LUMO energy levels. Figure 2c demonstrates that the calculated E_g values of these PCPs follow the same trend as the experimentally measured ones (Figure 2b). Both the HOMO and the LUMO energy levels for PDI-based PCP1 lie much deeper than donor chromophore-based PCPs. The introduction of bpy slightly lowered the energy levels due to its stronger electron-withdrawing ability as compared to bph unit (Figure 2d). In this work, the trans-configuration of bpy unit was assumed for all DFT calculations due to its higher thermodynamic stability as compared to that of the *cis*-configuration.[27,28] Molecular orbital diagrams (Figures S10 and S11) indicate that bpy unit presents a coplanar structure and the LUMO orbitals spread more onto the bpy unit than the bph unit. It is also clear that the HOMO of the model repeating unit of PCP2e and PCP4e is mostly localized on M_2 and M_4 units and LUMO is extended into the bpy unit, indicating the internal polarization.

Photocatalytic Hydrogen Production. Photocatalytic hydrogen production experiments were carried out with these PCPs in the presence of a sacrificial agent (SA). For the initial test, no additional metal cocatalyst was added. Solar simulator equipped with a 150 W xenon lamp was used as the light source, and two cooling fans were used to keep the reaction cell at room temperature (Figure S12). Methanol, diethanolamine (DEOA), diethylamine (DEA), and triethylamine (TEA) were used as sacrificial agents. The best performance of all PCPya photocatalysts was achieved by using TEA as sacrificial agent with the following order of the measured PHP rates: TEA > DEA > DEOA > methanol (Figure S13). It was found that the amine/water solutions can better wet a given PCP photocatalyst (Figure S14). The bpy-containing PCPye shows even better wettability in amine/water solutions than the corresponding bph-containing PCPye (Figure S15). A linear relation between the reaction time under full arc irradiation and the produced hydrogen amount was observed with PCP4e within 9 h (Figure S16), indicating a steady hydrogen production process. Experiments with different PCP4e concentrations (from 1.0 to 5.0 mg/mL) showed a limited enhancement (1.2 times higher) of hydrogen production rate (Figure S17), indicating the concentration of photocatalyst is high enough to utilize the incident photons. No obvious induction period was observed for these PCP photocatalysts. FTIR and diffuse reflectance UV−vis spectra of the PCP4e photocatalyst before and after the photoreaction show no obvious implication of photodegradation (Figure S18). The recycling experiment by using fresh TEA/water mixture and recycled PCP4e (after 24 h irradiation) shows ∼75% of the initial hydrogen production rate was retained.

Figure 3a shows the dependence of hydrogen production rate on the bpy content, based on 3 h irradiation of all PCP photocatalysts. It was found that the photocatalytic activity can be greatly enhanced by increasing the bpy content. PCP4e shows the best performance (33.0 μmol/h) with a ∼5 times enhancement as compared to PCP4a. The overall performance follows the order as PCP4 > PCP2 > PCP3 > PCP1. This trend seems to be consistent with the degree of extended conjugation allowed by the chemical structures. It is worth noting that the visible light absorption of PDI-based PCPs is not improved by the introduction of bpy comonomer due to minimal charge transfer feature between electron-deficient PDI and bpy units.

DOI: 10.1021/jacs.6b03472
J. Am. Chem. Soc. 2016, 138, 7681−7686

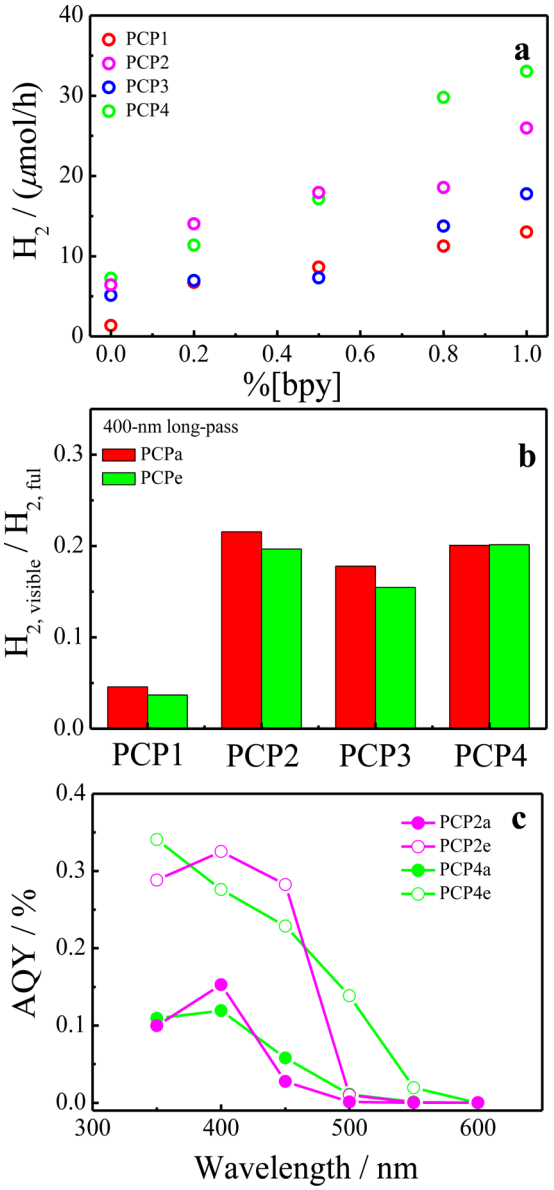

Figure 3. (a) Photocatalytic hydrogen production rates of PCPs with different bpy contents under full-arc irradiation. (b) Retention ratios of photocatalytic hydrogen production rates of PCPs under visible light and full-arc irradiation, where $H_{2,visible}$ and $H_{2,ful}$ represent the rate under visible light and full-arc illumination. (c) Wavelength-dependent apparent quantum yields (AQY) for PCP2a, PCP2e, PCP4a, and PCP4e.

Therefore, the observed PHP rate enhancement of PDI-based PCP1 implies that the bpy played an important role other than light absorption. The nitrogen atom in the bpy may interact with H_2O molecules through hydrogen-bonding interaction, which can help increase the local concentration of water molecules for water reduction.

The visible-light activity of these PCPs was further investigated by using a long-pass filter that only transmits visible light (λ > 400 nm). The optical characterization of bandpass and long-pass filters used in this study was shown in Figure S19. It was found that the photocatalytic rate was greatly reduced for all of the PCPs under only visible light illumination (Figure S20). A maximum rate of ~6.7 μmol/h was achieved by PCP4e. Figure 3b shows the retention ratios of photocatalytic hydrogen production rates of PCPs under visible light and full-arc irradiation. The donor-chromophore-based PCPs showed a stronger visible light activity with a retention ratio (~20%) than PDI-based PCPs (~5%). The difference of retention ratios probably reflected the contribution of internal polarization that favors charge separation and fully conjugated network that favors charge transport. This hypothesis needs further detailed studies by using the ultrafast spectroscopic technique.

Apparent Quantum Yield (AQY). The apparent quantum yields (AQY) of the two most efficient PCP photocatalysts (PCP2 and PCP4) were measured as a function of the incident light wavelength. The results are summarized in Figure 3c. For PCPe photocatalysts, AQY decreases as wavelength increases in the visible light range, and the longest wavelength capable of inducing hydrogen production coincided with the absorption onsets of the PCPe photocatalysts (Figure S8). The PCP4e shows a considerable visible light activity at wavelength as long as ~550 nm due to its better light absorption ability and charge transport property (ordered structure), while PCP2e started to show considerable activity only when the wavelength reaches ~450 nm. The highest AQY of 0.34% was achieved for PCP4e at 350 nm. In contrast, AQYs for bph-containing PCPa photocatalysts show 3−5 times reduced catalytic activity for a given wavelength as compared to those of PCPe photocatalysts. Moreover, the wavelength for efficient hydrogen production was reduced to 450 nm due to the limited light absorption ability of PCPa photocatalysts.

Effect of the Residual Pd on the PHP Performance. Most semiconductors cannot give high H_2 evolution activities without a metal cocatalyst even in the presence of sacrificial electron donor. The main reason is the facile recombination of electron−hole pairs before migrating to the surface for reactions.[29−31] In the work described here so far, no additional noble metal cocatalysts were added for the hydrogen production from water. Similar phenomenon was previously observed by Cooper et al.[16] The considerable PHP activities of these PCPs and the enhancement of reaction rate by the introduction of bpy moiety led us to rethink the effect of the residual metal palladium (Pd) introduced during the Pd-catalyzed polycondensation process on the photocatalytic activity. Figure 4a shows the ICP-MS results of the Pd contents of these PCP photocatalysts. It was observed that the residual Pd concentration is significant and ranges from 0.8−1.9 wt % for these PCPs. However, positive correlation between the hydrogen production rate and the residual Pd content was not found for these PCPs. These findings seem to suggest that the residual Pd has no significant effect on the rate of hydrogen production.

However, the previous studies on the effect of residual metal on the performance of organic photovoltaic devices (OPVs) indicated that the residual metal with a content as low as 0.01−0.1 wt % had a fatal influence on the performance of OPV devices.[32−34] Thus, we moved to study how the initial feeding ratio ([Pd]/[M]) of $Pd(PPh_3)_4$ catalyst and monomer affects the photocatalytic activity of the prepared PCP4e. ICP-MS study shows that the residual Pd content increases from 0.04% to 1.88% as the initial [Pd]/[M] ratio changes from 0.005 to 0.40 (Figure S21). The photocatalytic study (Figure 4b) shows the PHP rate increases rapidly as the residual metal content increases from 0.04% to 0.46%, and becomes saturated at higher Pd content. A threshold [Pd]/[M] ratio around 0.08 was observed. This result suggests that the residual Pd may still acts as cocatalyst in PHP reaction and answers why no correlation

DOI: 10.1021/jacs.6b03472
J. Am. Chem. Soc. 2016, 138, 7681−7686

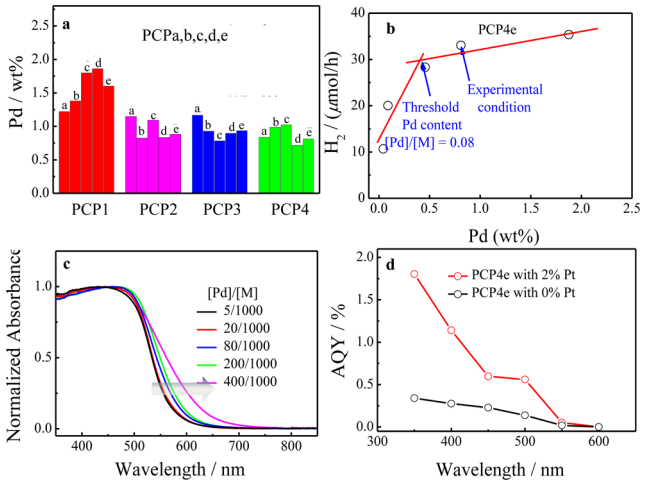

Figure 4. (a) Residual Pd contents for PCPs measured by ICP-MS. (b) Residual Pd content dependence of hydrogen production rate by using PCP4e as photocatalyst. (c) Diffuse reflectance UV−vis absorption spectra of these PCP4e photocatalysts prepared with different [Pd]/[M] ratios. (d) Wavelength-dependent apparent quantum yield (AQY) for PCP4e with different Pt loading.

between the hydrogen production rates and the Pd residual contents was found in Figure 4a, simply because the photocatalytic activity of PCPs gets saturated when the residual Pd content reaches the threshold. This phenomenon of metal cocatalyst threshold was also observed in the previous studies on the photocatalyst based on inorganic semiconductor PdS/CdS[35] and La-doped $NaTaO_3$,[36] where 0.2 wt % Pt and 1.0 wt % Au were found to be the thresholds, respectively.

We understand that when the catalyst concentration for polymerization changes, degree of polymerization may also change, which will affect the optical properties of the resulting materials. To explore the effect of band structure on the photocatalytic performance, diffuse reflectance UV−vis spectroscopy measurements of these PCP4e prepared with different amounts of $Pd(PPh_3)_4$ catalyst were carried out. The results (Figure 4c) show that the absorption onset indeed gradually shifts to longer wavelength as initial [Pd]/[M] increases, indicating that a better conjugation of PCP can probably be achieved at higher Pd catalyst loading. However, this Pd content-dependent red-shift may also be originated from the enhanced polymer-to-metal charge transfer feature and coordination of Pd with bpy moiety. Overall, the increase of [Pd]/[M] from 0.005 to 0.2 led to slight red-shift but 3 times increase of photocatalytic activity, while the increase of [Pd]/[M] from 0.2 to 0.4 led to an obvious red-shift but only slight enhancement of photocatalytic activity, which implies that the amount of residual Pd, as compared to the energy bandgap, may be the more important factor for determining the photocatalytic activity of a given PCP photocatalyst.

It is well-known that the Pd residues in linear conjugated polymers can be lowered to 0.1−1.0 ppm (10^{-6} wt %) by EDTA and Soxhlet extraction purification procedure.[32,34,37] The removal of Pd is much more difficult for PCPs because of the cross-linked and porous structures, which may help spatially trap the Pd nanoparticles formed during the polymerization process. Attempts at removing the residual Pd of PCP4e were made in EDTA (saturated) or HCl (1 M) solution at 80 °C for 12 h, but no obvious decrease of the Pd content and the corresponding photocatalytic activity was observed (Figure S22). The color change of PCP4e from orange to red upon the HCl treatment indicated the protonation of pyridine units occurred. In contrast, control experiment of adding $CoCl_2$, which is supposed to coordinate with ligand bpy, did not result in a color change of the solution, implying the failure of the metal−ligand coordination. This observation further supports our conjecture that the bpy moieties exist in the *trans*-configuration.

To further probe the effect of metal cocatalysts, we tested the PHP performance of PCP4e loaded with 2 wt % platinum (Pt) by photodeposition from K_2PtCl_6 because Pt is proved to be one of the state-of-art noble metal cocatalysts for hydrogen evolution. The result shows that an enhancement of ∼5 times in the PHP activity rate was achieved upon loading Pt cocatalyst, and an AQY as high as 1.80% was obtained at 350 nm (Figure 4d), further demonstrating the importance of metal cocatalyst for achieving high photocatalytic performance.

Effect of the Comonomer on the PHP Performance. An intriguing question is the function of nitrogen site in the pyridine ring. To gain more insight, polymers PCP5−7 were successfully prepared (Figure 5a, Figures S23 and S24) and

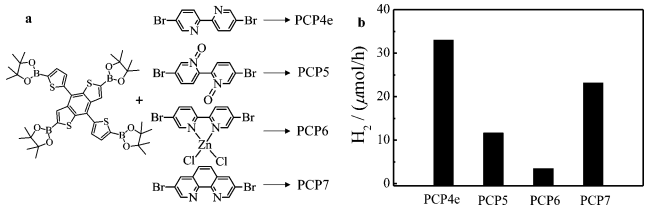

Figure 5. (a) Structures of monomers and synthesis of PCP5−7 photocatalysts by Suzuki polycondensation. (b) Photocatalytic hydrogen production rates of PCP4e and PCP5−7 under full-arc irradiation.

used as photocatalysts. Because of the nonplanar structure of bipyridine-dioxide, a blue shift of absorption onset was observed for PCP5, while red shift of absorption onsets was observed for PCP6 and PCP7 because of the enhanced push−pull effect (Figure S24a). As compared to PCP4e, PCP7 shows a longer absorption edge (650 nm), which results in a better light absorption but a decrease of redox potential for proton reduction; moreover, the internal dipole orientation is different for bipyridine (*trans*) and phenanthroline (*cis*). PHP test results (Figure 5b) of these polymers show that a relatively high PHP efficiency was observed for PCP7-containing bare nitrogen atoms, while the block of nitrogen sites led to a significant decrease of the PHP rates for PCP5 and PCP6. Results imply that the introduction of weak acceptor bpy can enhance the efficiency of PCP photocatalysts by improving light absorption, interfacial wettability, and the charge separation and transport processes. More detailed studies on this issue need ultrafast spectroscopic measurements and will be discussed by due time.

CONCLUSIONS

A series of porous conjugated polymers (PCPs) with varied chromophore and bipyridyl (bpy) contents were synthesized and found to evolve hydrogen photocatalytically from water. It was found that the PHP activity of coplanar bpy-containing PCPs can be greatly enhanced due to the improved light absorption, better wettability, and the improved charge separation processes. Those PCPs containing donor monomer DBD (M_4) with fully conjugated backbone and ordered local structure showed highest activity, indicating the importance of

DOI: 10.1021/jacs.6b03472
J. Am. Chem. Soc. 2016, 138, 7681−7686

charge transport. This study also suggests the residual palladium plays a key role for the catalytic performance, and the performance of PCP photocatalyst can be further improved by loading 2 wt % of platinum.

■ ASSOCIATED CONTENT

Supporting Information

The Supporting Information is available free of charge on the ACS Publications website at DOI: 10.1021/jacs.6b03472.

Full experimental methods, supporting Figures S1−24, Table S1, and NMR and UV−vis spectra of monomers (PDF)

■ AUTHOR INFORMATION

Corresponding Author

*lupingyu@uchicago.edu

Notes

The authors declare no competing financial interest.

■ ACKNOWLEDGMENTS

This work is supported by the National Science Foundation (DMR-1263006 and NSF- SEP-1229089, LPY) and by the U.S. Department of Energy, Office of Science, Office of Basic Energy Sciences, through Argonne National Laboratory under contract no. DE-AC02-06CH11357. This work also benefited from NSF MRSEC at the University of Chicago.

■ REFERENCES

(1) Artero, V.; Chavarot-Kerlidou, M.; Fontecave, M. *Angew. Chem., Int. Ed.* **2011**, *50*, 7238.
(2) Kudo, A.; Miseki, Y. *Chem. Soc. Rev.* **2009**, *38*, 253.
(3) Moniz, S. J. A.; Shevlin, S. A.; Martin, D. J.; Guo, Z. X.; Tang, J. *Energy Environ. Sci.* **2015**, *8*, 731.
(4) Wang, X.; Maeda, K.; Thomas, A.; Takanabe, K.; Xin, G.; Carlsson, J. M.; Domen, K.; Antonietti, M. *Nat. Mater.* **2009**, *8*, 76.
(5) Liu, J.; Liu, Y.; Liu, N.; Han, Y.; Zhang, X.; Huang, H.; Lifshitz, Y.; Lee, S. T.; Zhong, J.; Kang, Z. *Science* **2015**, *347*, 970.
(6) Martin, D. J.; Qiu, K.; Shevlin, S. A.; Handoko, A. D.; Chen, X.; Guo, Z.; Tang, J. *Angew. Chem., Int. Ed.* **2014**, *53*, 9240.
(7) Wang, Y.; Di, Y.; Antonietti, M.; Li, H.; Chen, X.; Wang, X. *Chem. Mater.* **2010**, *22*, 5119.
(8) Zhang, J.; Zhang, G.; Chen, X.; Lin, S.; Möhlmann, L.; Dołęga, G.; Lipner, G.; Antonietti, M.; Blechert, S.; Wang, X. *Angew. Chem., Int. Ed.* **2012**, *51*, 3183.
(9) Kailasam, K.; Mesch, M. B.; Möhlmann, L.; Baar, M.; Blechert, S.; Schwarze, M.; Schröder, M.; Schomäcker, R.; Senker, J.; Thomas, A. *Energy Technol.* **2016**, n/a.
(10) Schwab, M. G.; Hamburger, M.; Feng, X.; Shu, J.; Spiess, H. W.; Wang, X.; Antonietti, M.; Mullen, K. *Chem. Commun.* **2010**, *46*, 8932.
(11) Zhang, Z.; Long, J.; Yang, L.; Chen, W.; Dai, W.; Fu, X.; Wang, X. *Chem. Sci.* **2011**, *2*, 1826.
(12) Kailasam, K.; Schmidt, J.; Bildirir, H.; Zhang, G.; Blechert, S.; Wang, X.; Thomas, A. *Macromol. Rapid Commun.* **2013**, *34*, 1008.
(13) Stegbauer, L.; Schwinghammer, K.; Lotsch, B. V. *Chem. Sci.* **2014**, *5*, 2789.
(14) Yanagida, S.; Kabumoto, A.; Mizumoto, K.; Pac, C.; Yoshino, K. *J. Chem. Soc., Chem. Commun.* **1985**, 474.
(15) Shibata, T.; Kabumoto, A.; Shiragami, T.; Ishitani, O.; Pac, C.; Yanagida, S. *J. Phys. Chem.* **1990**, *94*, 2068.
(16) Sprick, R. S.; Jiang, J. X.; Bonill, o B.; Ren, S.; Ratvijitvech, T.; Guiglion, P.; Zwijnenburg, M. A.; Adams, D. J.; Cooper, A. I. *J. Am. Chem. Soc.* **2015**, *137*, 3265.
(17) Vyas, V. S.; Haase, F.; Stegbauer, L.; Savasci, G.; Podjaski, F.; Ochsenfeld, C.; Lotsch, B. V. *Nat. Commun.* **2015**, *6*, 8508.
(18) Thote, J.; Aiyappa, H. B.; Deshpande, A.; Díaz Díaz, D.; Kurungot, S.; Banerjee, R. *Chem. - Eur. J.* **2014**, *20* (48), 15961.
(19) Wang, Z.; Yuan, S.; Mason, A.; Reprogle, B.; Liu, D.-J.; Yu, L. *Macromolecules* **2012**, *45*, 7413.
(20) Xia, J.; Yuan, S.; Wang, Z.; Kirklin, S.; Dorney, B.; Liu, D. J.; Yu, L. *Macromolecules* **2010**, *43*, 3325.
(21) Yuan, S.; Kirklin, S.; Dorney, B.; Liu, D. J.; Yu, L. *Macromolecules* **2009**, *42*, 1554.
(22) Yuan, S.; Shui, J. L.; Grabstanowicz, L.; Chen, C.; Commet, S.; Reprogle, B.; Xu, T.; Yu, L.; Liu, D. J. *Angew. Chem., Int. Ed.* **2013**, *52*, 8349.
(23) Carsten, B.; Szarko, J. M.; Lu, L.; Son, H. J.; He, F.; Botros, Y. Y.; Chen, L. X.; Yu, L. *Macromolecules* **2012**, *45*, 6390.
(24) Jung, I. H.; Lo, W. Y.; Jang, J.; Chen, W.; Zhao, D.; Landry, E. S.; Lu, L.; Talapin, D. V.; Yu, L. *Chem. Mater.* **2014**, *26*, 3450.
(25) Son, H. J.; Wang, W.; Xu, T.; Liang, Y.; Wu, Y.; Li, G.; Yu, L. *J. Am. Chem. Soc.* **2011**, *133*, 1885.
(26) Weber, J.; Antonietti, M.; Thomas, A. *Macromolecules* **2008**, *41*, 2880.
(27) Göller, A.; Grummt, U. W. *Chem. Phys. Lett.* **2000**, *321*, 399.
(28) Nakamoto, K. *J. Phys. Chem.* **1960**, *64*, 1420.
(29) Cao, S.; Low, J.; Yu, J.; Jaroniec, M. *Adv. Mater.* **2015**, *27*, 2150.
(30) Thoi, V. S.; Sun, Y.; Long, J. R.; Chang, C. J. *Chem. Soc. Rev.* **2013**, *42*, 2388.
(31) Yang, J.; Wang, D.; Han, H.; Li, C. *Acc. Chem. Res.* **2013**, *46*, 1900.
(32) Bracher, C.; Yi, H.; Scarratt, N. W.; Masters, R.; Pearson, A. J.; Rodenburg, C.; Iraqi, A.; Lidzey, D. G. *Org. Electron.* **2015**, *27*, 266.
(33) Krebs, F. C.; Nyberg, R. B.; Jørgensen, M. *Chem. Mater.* **2004**, *16*, 1313.
(34) Nikiforov, M. P.; Lai, B.; Chen, W.; Chen, S.; Schaller, R. D.; Strzalka, J.; Maser, J.; Darling, S. B. *Energy Environ. Sci.* **2013**, *6*, 1513.
(35) Yan, H.; Yang, J.; Ma, G.; Wu, G.; Zong, X.; Lei, Z.; Shi, J.; Li, C. *J. Catal.* **2009**, *266*, 165.
(36) Iwase, A.; Kato, H.; Kudo, A. *Appl. Catal., B* **2013**, *136−137*, 89.
(37) Nielsen, K. T.; Bechgaard, K.; Krebs, F. C. *Macromolecules* **2005**, *38*, 658.

DOI: 10.1021/jacs.6b03472
J. Am. Chem. Soc. 2016, 138, 7681−7686